

Data science for understanding physics – modelling detectability of ship wake components using machine learning

Björn Tings*, Karl Kortum

German Aerospace Center (DLR), Remote Sensing Technology Institute Bremen
*bjorn.tings@dlr.de

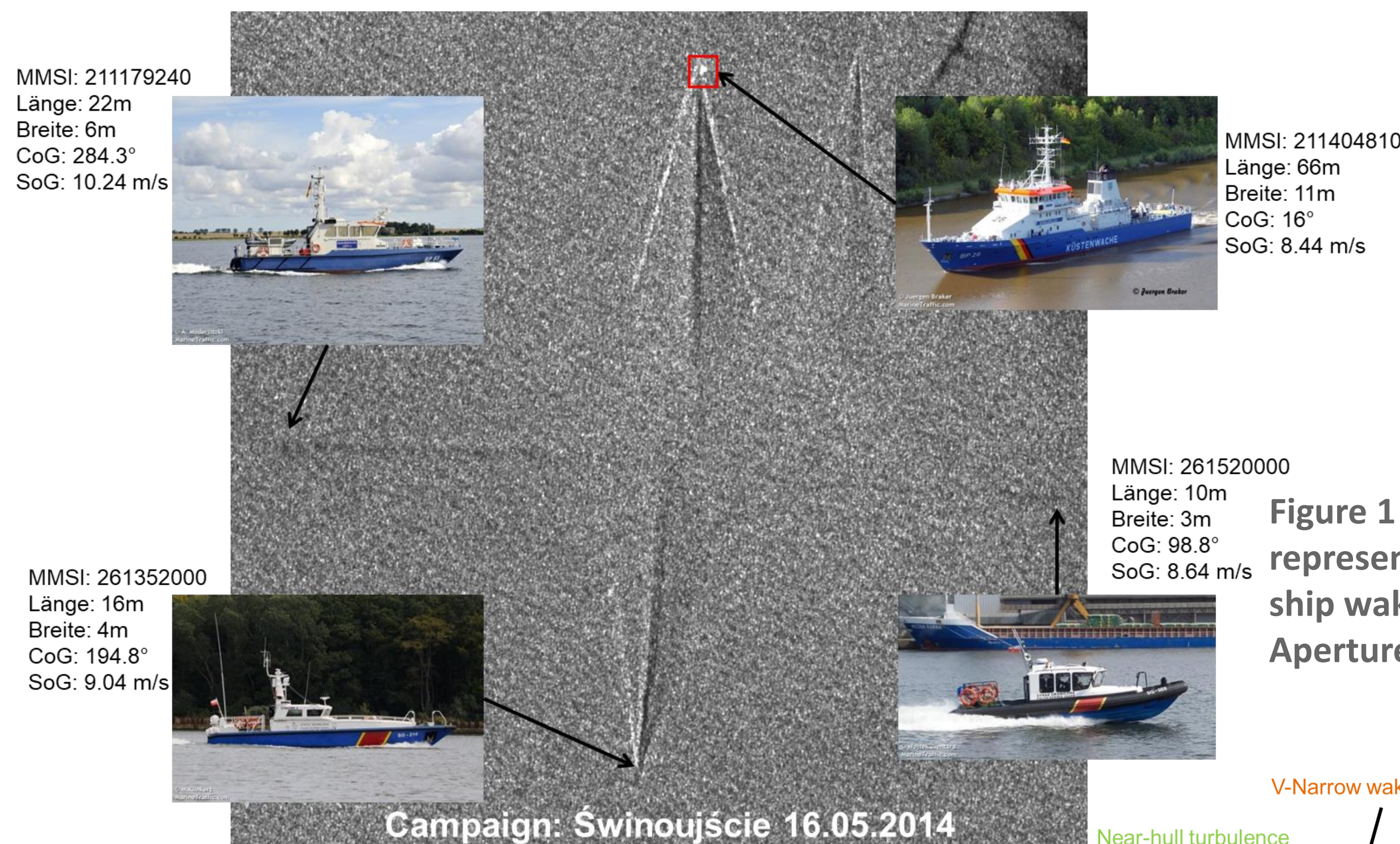


Figure 1 (top left): Motivation for this study is provided by a campaign in 2014 with Polish Coast Guard and Federal Police Sea. The wakes generated by vessels with movement parallel to Range direction (horizontal) are worse detectable than wake generated by vessels with movement parallel to Azimuth direction (vertical).

Introduction & Motivation

Ship wakes consists of multiple components, which are detectable in acquisitions from satelliteborne Synthetic Aperture Radar (SAR) sensors. Their detectability varies in dependency to influencing parameters, which can be categorized into the types: environmental parameters, image acquisition settings and ship properties. An example of varying detectability of ship wakes and a schematic representation of detectable wake components are presented in Figure 1. In this study, machine learning (i.e. Support Vector Regression (SVR)) is used to model the dependency between nine influencing parameters and the detectability of individual wake components.

Data

SAR data from four satellite SAR missions is used. The SAR datasets with in total 4000 wake samples are summarized in Table 1. The nine influencing parameters affecting the detectability of each of the wake samples are described in Table 2. The length of each wake component is measured, based on a manual retracing of the wake component's outlines. The plots in Figure 2 a) provide an exemplary view into the feature space spanned by two of the influencing parameters with length of a wake component, which is indicating the respective wake component's detectability.

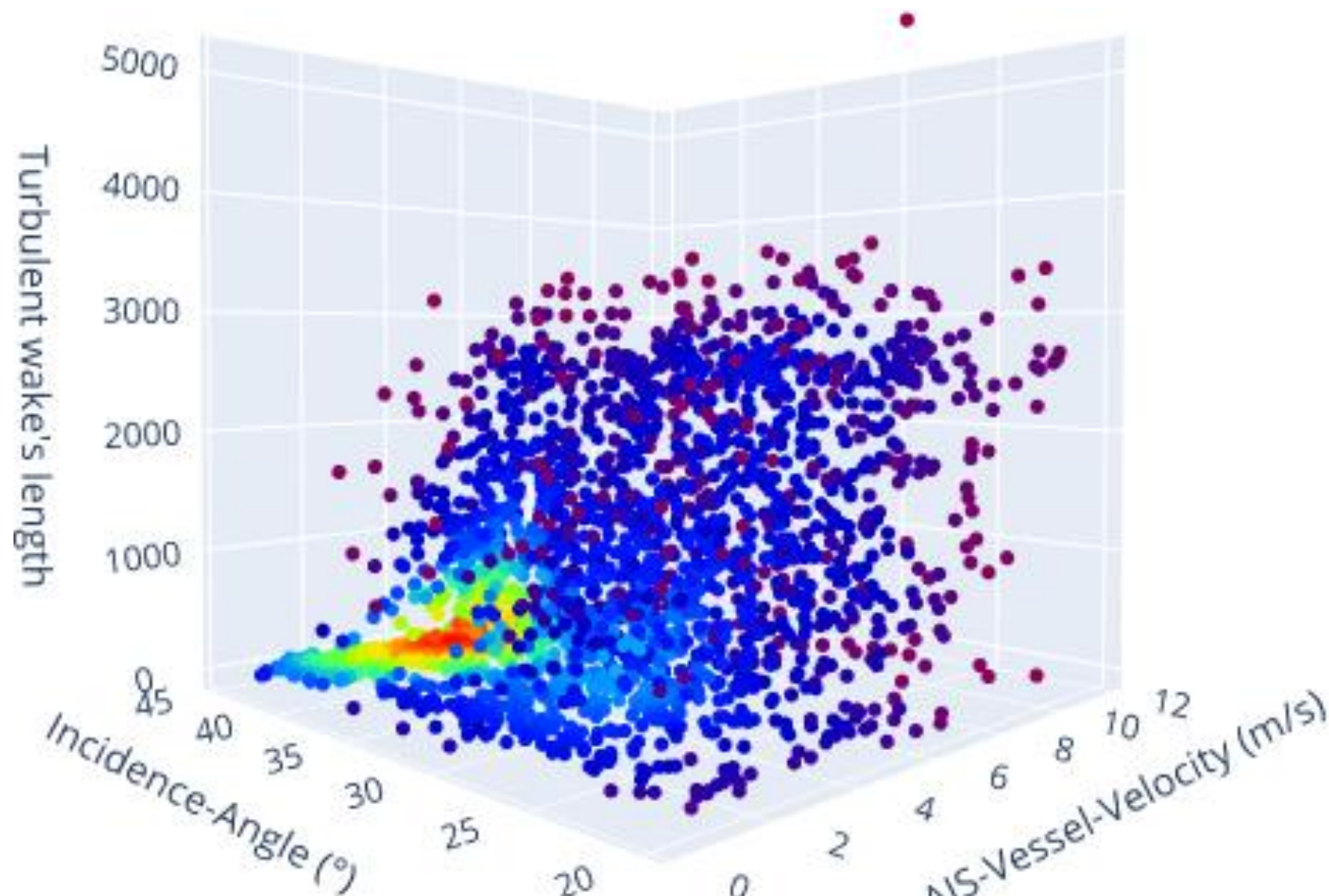


Figure 2 a): Feature space with all wake samples of TSX dataset for two influencing parameters and wake length

Table 1: Summary of SAR datasets for SAR missions TerraSAR-X (TSX), CosmoSkymed (CSK), Sentinel-1 (S1) and RADARSAT-2 (RS2)

	TSX	CSK	S1	RS2
Frequency band	X	X	C	C
Acquisitions modes	SL, SM	HI	IW	MF, F, S
Amount of products	1097	11	31	53
Amount of wake samples	2881	94	618	407

Table 2: List of nine influencing parameters investigated with respect to their influence on the detectability of individual wake components.

Nr i,	Influencing Parameter Name (x_i)	Description
1	AIS-Vessel-Velocity (x_1)	Velocity of the vessel derived from AIS
2	AIS-Length (x_2)	Length of the vessel derived from AIS
3	AIS-CoG (x_3)	Course over ground (CoG) derived from AIS relative to the radar looking direction
4	Incidence-Angle (x_4)	Incidence angle of the radar
5	SAR-Wind-Speed (x_5)	Wind speed estimated from SAR backscatter of ocean background
6	SAR-Significant-Wave-Height (x_6)	Significant wave height estimated from SAR backscatter of ocean background
7	SAR-Wave-Length (x_7)	Wavelength estimated from from SAR backscatter of ocean background
8	AIS-CoG-SAR-Wave-Direction (x_8)	Absolute angular difference between AIS-CoG and wave direction estimated from SAR backscatter of ocean background
9	AIS-CoG-WRF-Wind-Direction (x_9)	Absolute angular difference between AIS-CoG and wind direction estimated by the Weather Research and Forecasting Model (WRF)

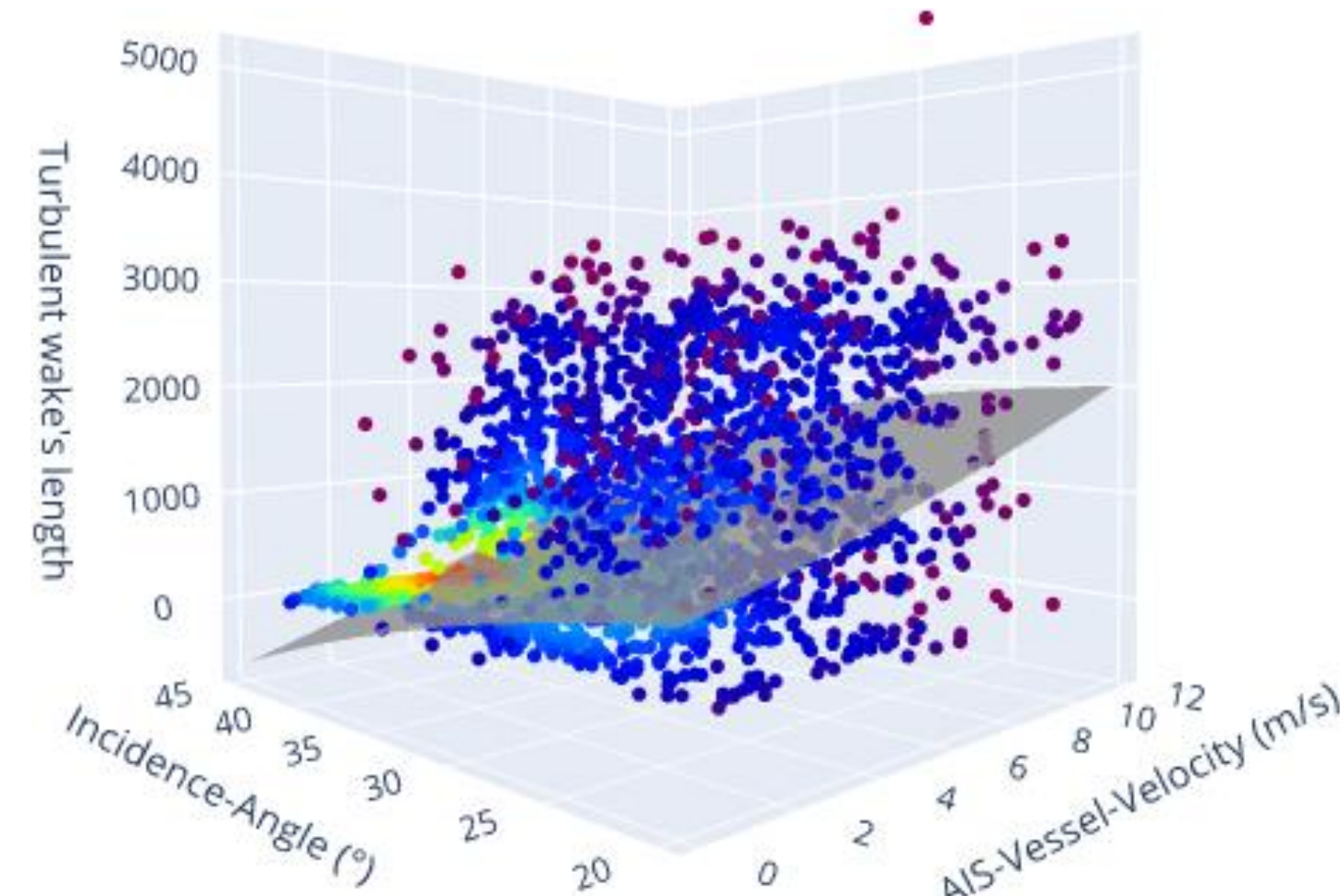


Figure 2 b): Gray hyperplane visualizing detectability model for turbulent wakes based on displayed wake samples

Method

In order to investigate the detectability of a wake component w , a normalized figure of merit for wake detectability is required. In this study, the indicator of detectability, i.e. wake component length, is normalized between a minimum and maximum length boundary to obtain the so called Detectable Length Metric (DLM). A SVR model f_w for mapping DLM_w to the influencing parameters x_i is trained:

$$DLM_w = f_w(x_1; x_2; x_3; x_4; x_5; x_6; x_7; x_8; x_9)$$

In Figure 2 b) an example of f_w for turbulent wakes is visualized by the gray hyperplane. By sampling the whole nine-dimensional feature space of by discretized values for x_i and ingesting f_w using each discretized tuple, DLM_w values for each possible detection condition are calculated. After colour-coding DLM_w heatmaps can be generated as shown in Figure 3. Those heatmaps give insight into the dependency between the influencing parameters and the detectability of a wake component.

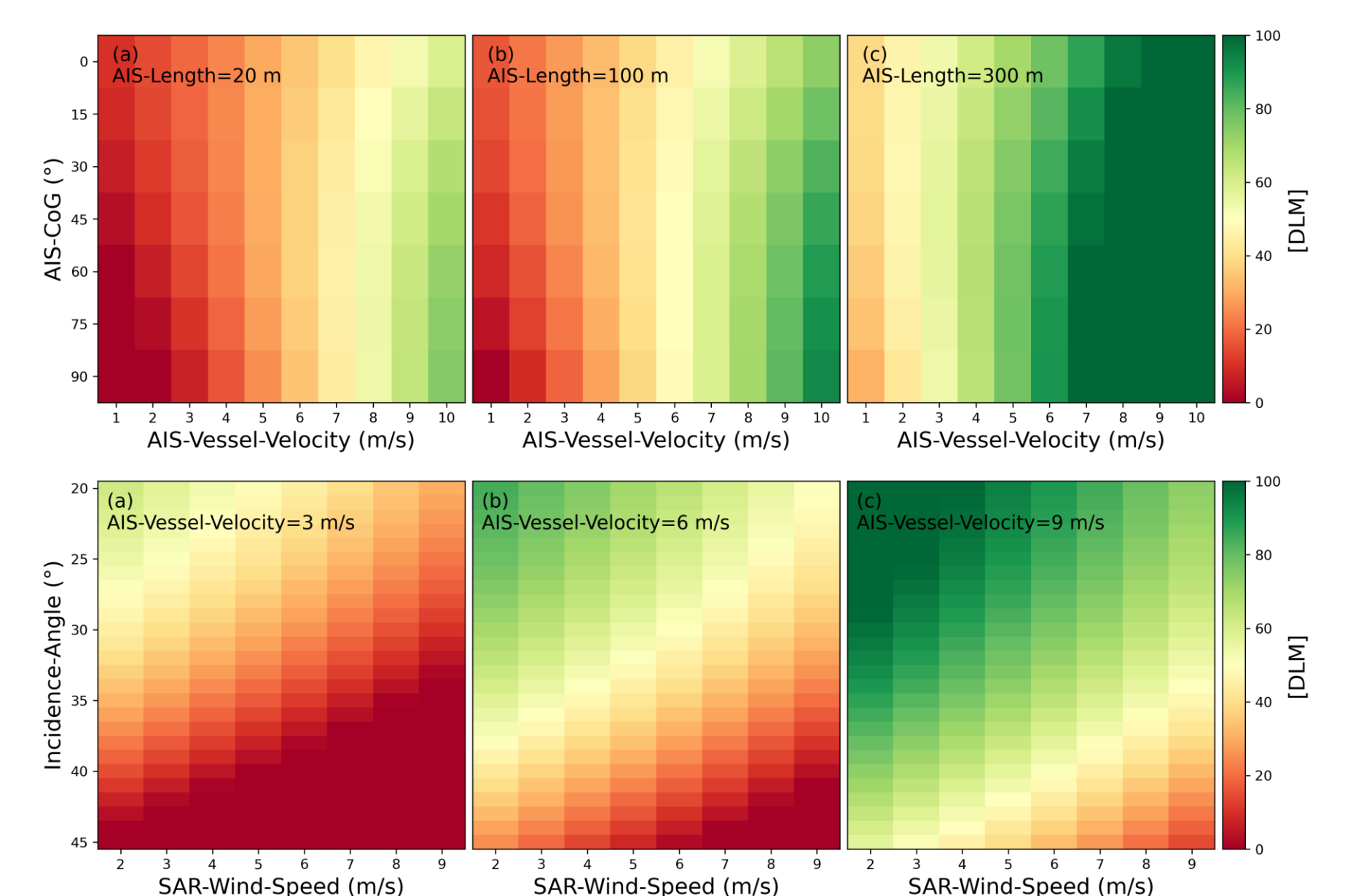


Figure 3: Heatmaps for detectability of turbulent wakes

By contrasting detectability models generated for different sensors, the overall performance of different SAR missions with respect to the task of wake detection can be compared. The contrasting of several models is visualized in Figure 2 c), where multiple models for two sensors are visualized by hyperplanes with two shades of gray (light gray for TSX and dark gray for CSK).

Conclusion

The statements on wake detectability derived from the detectability models are in agreement with literature on wake recognition using simulations and/or physical contemplation. Further can be concluded from the available data that X-band SAR sensors are better suited for detection of Kelvin wake arms and V-narrow wakes than C-band SAR sensors. Not only the output of machine learning models is of scientific value. Also the model composition itself can be investigated for gaining knowledge of physical relationships.

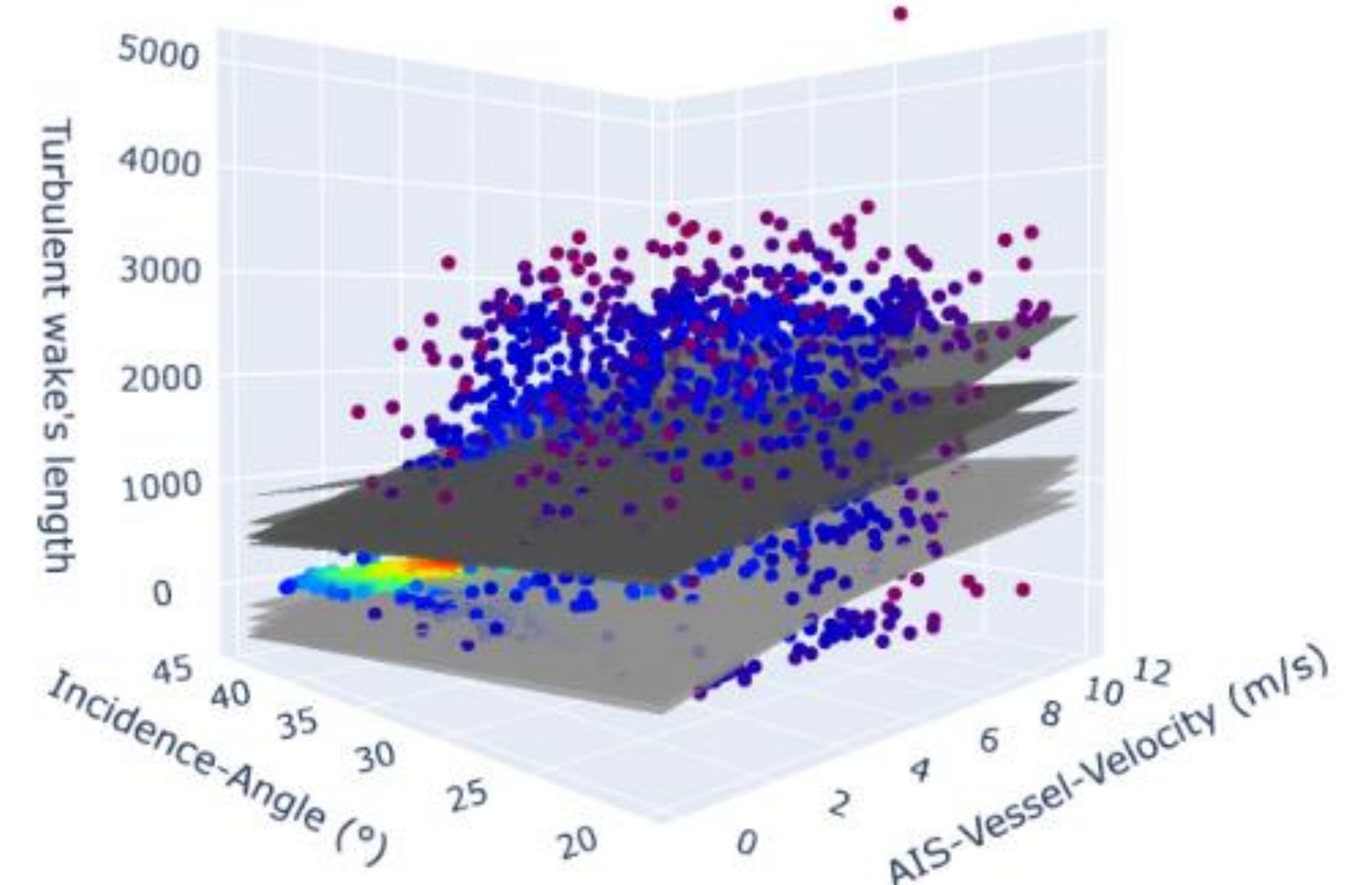


Figure 2 c): Comparison of models build for five data subsets each for TSX (light gray) and CSK (dark gray)

Acknowledgments: Data provided by the European Space Agency. Produced using COSMO-SkyMed satellite image © ASI (2018 - 2019), provided by e-GEOS under ESA's TPM scheme. RADARSAT is an official mark of the Canadian Space Agency.

References:

- B. Tings, "Non-Linear Modeling of Detectability of Ship Wake Components in Dependency to Influencing Parameters Using Spaceborne X-Band SAR," Remote Sensing, vol. 13, no. 2, p. 165, 2021.
B. Tings, A. Pleskachevsky and S. Wiehle, "Comparison of detectability of ship wake components between C-Band and X-Band synthetic aperture radar sensors operating under different slant ranges," ISPRS Journal of Photogrammetry and Remote Sensing, vol. 196, pp. 306-324, 2023.